Fabrication of RGO/Cu composites based on electrostatic adsorption

Wen-min ZHAO[1], Rui BAO[1,2*,3], Jian-hong Yi[1,2*], Xiang-hui HOU[3], Dong FANG[1], Chun-xuan LIU[4]

1. Faculty of Materials Science and Engineering, Kunming University of Science and Technology, Kunming 650093, China

2. Key Laboratory of Advanced Materials of Yunnan Province, Kunming 650093, China

3. Faculty of Engineering, University of Nottingham, University Park, Nottingham NG7 2RD, UK

4. Hunan Xiangtou Goldsky Technology Group Co. LTD., Changsha 410012, China

Corresponding author.

E-mail: baorui@kmust.edu.cn (Rui Bao)

E-mail: yijianhong@kmust.edu.cn (Jianhong Yi)

Abstract

To address the issues of reduced graphene oxide (RGO) dispersion in copper (Cu) matrix and interface bonding between RGO and Cu, an electrostatic adsorption method with interface transition phase design was employed to prepare the RGO/Cu based composites. Cu−Ti alloy powder was employed to improve the combination by forming carbides at the RGO−Cu interface. It was noted that the mechanical property of 0.3wt.%RGO/Cu−Ti composite was increased by 60% compared with that of the matrix. Strengthening mechanism analysis suggested that the enhancement of the mechanical property was ascribed to the load transfer and second phase strengthening which were from the improved dispersion of RGO and the in-situ formed titanium carbide phase.

Keywords:

Graphene oxide (GO);

Electrostatic adsorption;

Cu-Ti;

In-situ Ti_xC_y;

Mechanical properties

1. Introduction

Applications of graphene oxide (GO) or reduced graphene oxide (RGO) in metal matrix composites (MMCs), which offer excellent mechanical properties and comprehensive performance, have received considerable concern in recent years [1,2]. Conventional preparation methods have certain limitations to address the problems faced in preparing RGO/MMCs, which include uniform dispersion of graphene (GR) reinforcement in metal matrix without agglomeration and strong interface bonding between carbon strengthening phase and the metal matrix [1,3].

Uniform dispersion and distribution of GR in metal matrix are essential to improve the properties of MMCs [4, 5]. Electrostatic adsorption, a one-step method without the problem of introducing additional impurities, can be employed to disperse the GR in the copper matrix. This novelty method is built on the zeta potential difference between Cu and GR particles. A huge amount of chemical functional groups on the surface of GO give them hydrophilic properties and make them have a negative zeta potential in hydrochloric acid solution. At the same conditions, however, Cu powder has a positive zeta potential because of the weaker electronegativity Cu atom than that of chlorine atom. Hence, by adjusting and controlling the pH value of the solution where the two kinds of powders soaked in can attract them together with a well-dispersed and distributed GO [6].

However, GR has poor wettability with the Cu matrix, which is not beneficial to transfer the load efficiently. To improve the interface bonding, the third element atoms are usually added to form carbide at the interface. For example, graphite/Cu−Cr composites can generate chromium carbide to make the interface bond stronger [7,8]. However, limited attention is paid to the in-situ generated titanium−carbide reinforced copper based composites.

In this research, the electrostatic adsorption method for preparing composite powder was used. Then the interface bonding between Cu and RGO was investigated by using

Cu−Ti alloy powder to obtain an in-situ generated titanium−carbon transition phase. This experimental method had not been reported before. Due to the important influence of these compounds on the mechanical properties of RGO/Cu−Ti composites, the microstructure and strengthening mechanism of RGO/Cu−Ti composite were discussed underlying titanium−carbon compounds formation. Moreover, this research could effectively balance the integrity and dispersion of the composite enhanced phase (nanometer carbide phases and RGO phase) in the preparation, and achieve a good improvement in the mechanical performance of composite materials.

2. Experimental

When GO (or RGO) is introduced into the copper powders, the tendency of agglomeration between their powders should be conquered. Hence, we produced RGO/Cu composite powders by a simple electrostatic adsorption technique to enhance the dispersion of RGO in the Cu matrix. A schematic diagram of the fabrication process is given in Figure 1. First, the pretreated GOs (0.5-5 μm in lateral size and 0.8-1.2 nm in thickness) were dispersed in deionized water by ultrasonic for 15-20 minutes. At the same time, electrolytic Cu powder (99.9% pure, ~325 mesh in average particle size) was ball milled into the flaky shape and scattered in the deionized water under mechanical stirring. Next, the two suspensions were mixed together under the condition of continuous stirring, when the pH value of the Cu powder suspension was adjusted to ~4.0 by adding HCl solution. After filtering and drying, micro-sized GO/Cu_2O composite powder was prepared. As-prepared micro-sized GO/Cu_2O composite powder with different contents of GO was mixed with Cu-1.0wt.%Ti alloy powders using a low-energy ball milling. RGO/Cu-Ti composite powder was obtained by thermal reduction at 553 K for 6 hours with N_2+H_2. According to the nominal mass fraction of RGO in the mixed powder, the samples are marked as 0, 0.3%, 0.6% and 0.9%. Finally, the powders were sintered and densified by spark plasma sintering (SPS, LABOX-650F furnace). SPS was

operated at 1023 K under a vacuum atmosphere. Heating rate was 373 K min-1 and held at 1023 K for 10 min, it should be noted that it is necessary to maintain a pressure of 50 MPa from the start to the end of the sintering.

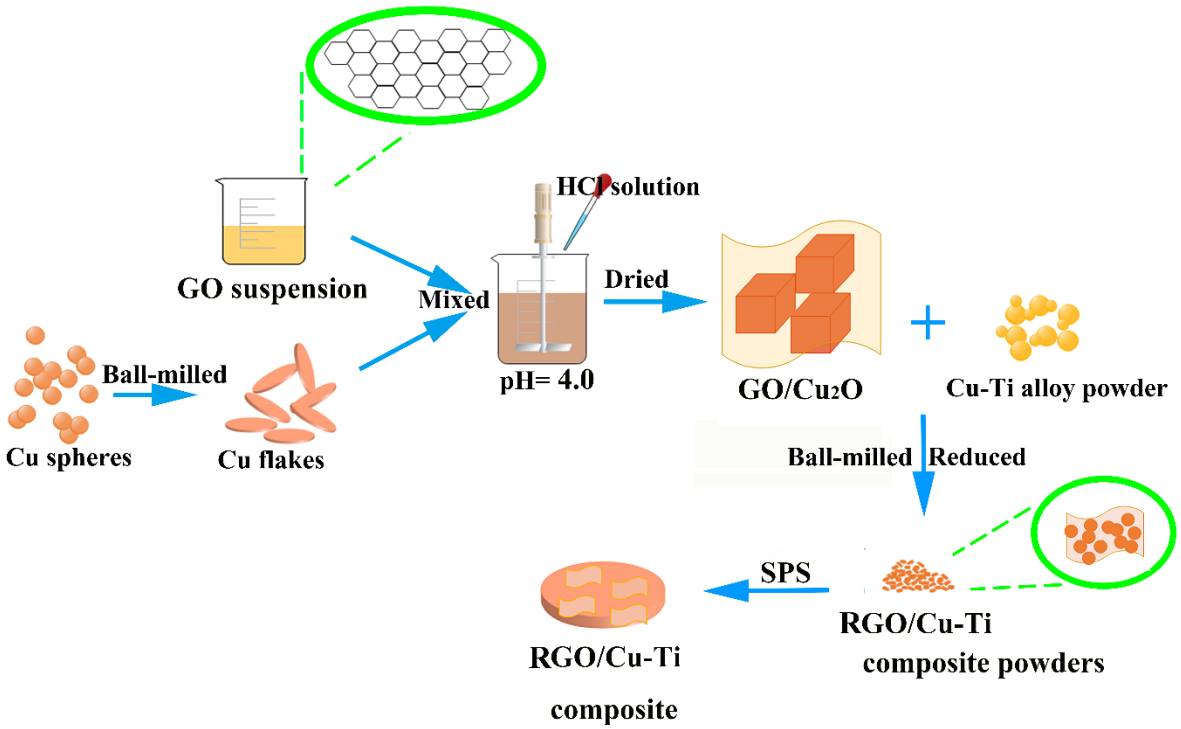

Figure 1. Schematic of fabrication process of RGO/Cu-Ti nanocomposite.

The functional group of the GO was characterized by Fourier transform infrared spectroscopy (FTIR; Nicolet IS10). The morphology and microstructure of RGO/Cu-Ti were obtained by Scanning electron microscopy (SEM, Nova Namo-450, FEI), transmission electron microscopy (HRTEM, Tecnai G2-TF30, S-Twin) and X-ray diffraction (XRD, RINT, Rigaku, Japan) with Cu K_{α} radiation. Structural defects in the GO and RGO/Cu-Ti composite powders were investigated using Raman spectroscopy (Labram HR Evolution, HORIBA JOBIN YVON Corp, French). The density of composites was evaluated according to the principle of Archimedes. Vickers microhardness of samples was measured by MC010 microhardness analysis system (Shanghai Microcre Light-Machine Tech Co. Ltd) with a load of 0.98N applied for 15s. Tensile test of RGO/Cu-Ti composites was conducted on

SHIMADZU equipment (AG-X plus, Japan) at ambient temperature with a tensile rate of 0.2 mm/min.

3. Result and discussion

3.1 Starting materials

Figure 2a illustrates the spherical Cu-1.0wt.%Ti alloy powder has a correspondingly wide size distribution of 1~50 μm, and EDS mapping images show that the uniformly distributed Ti element in the Cu-Ti alloy powders. TEM image of GO (Figure 2b) reveals a typical pleated sheet structure of GO. The functional groups of GO are identified according to the FTIR spectrum (Figure 2c), demonstrating the presence of C-O (~1118 cm^{-1}), C-H (~2924 cm^{-1}), O-H (~3450 cm^{-1}) and C=C (~1667 cm^{-1}) on the GO. These groups provide GO hydrophilic properties and showed a negative zeta potential under HCl conditions. On the contrary, Cu powder has a positive zeta potential because the Cu atom has weaker electronegativity than the chlorine atom in the same environment. This zeta potential difference of electrostatic adsorption between Cu and GO in theory[9, 10]. It is the presence of this positive and negative potential that binds the two together.

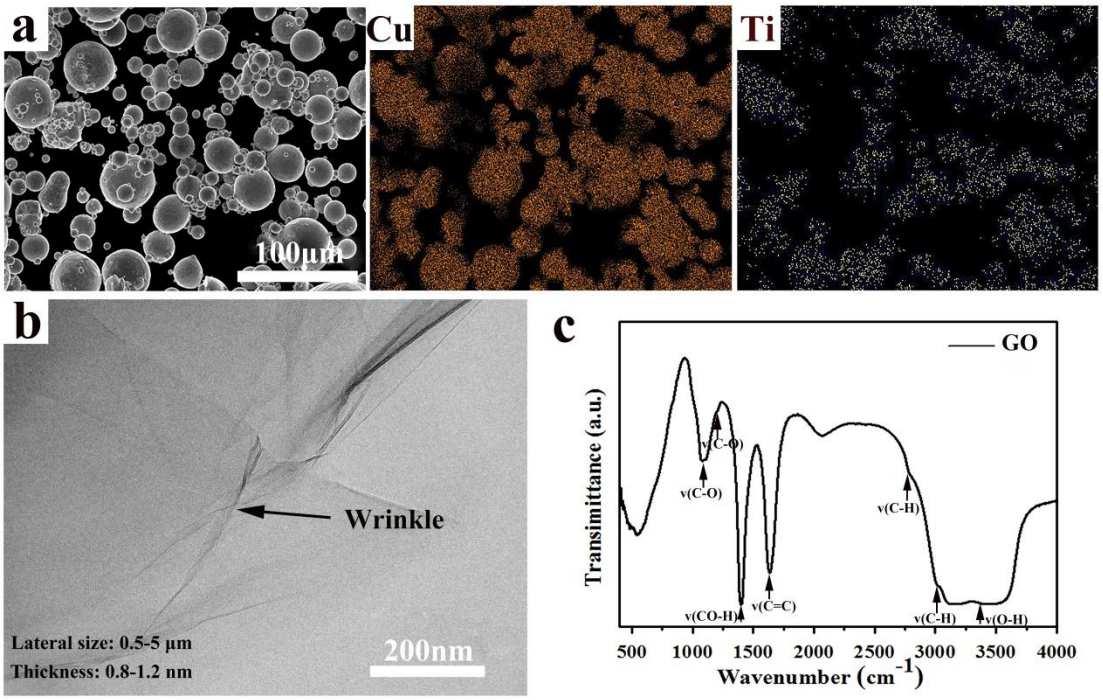

Figure 2. (a) Morphology and EDS mapping images of Cu-Ti alloy powder. (b) TEM image of GO. (c) FTIR spectrum of GO.

3.2 Composite powders

To increase the specific surface area, the spherical Cu powders were transformed into flake powders by the ball-milling process, which was beneficial for the adsorption of copper powder with GO (Figure 3a). Morphology of the GO/ Cu_2O composite powder prepared by electrostatic adsorption shows that all powders were turned into small block shape particles during the electrostatic adsorption and no flaked powder is observed, even though the process only lasted ~10 minutes (Figure 3b). Meanwhile, some Cu_2O powders were formed on both sides of the GO, suggesting a well-dispersed GO in the composite powders. Our previous studies have found that these cubic powders are cuprous oxide and the basic reaction principles and mechanism are discussed elsewhere [6]. And compared with[11-13] , it was found that by first synthesizing the GO/Cu_2O composite powder instead using the GO directly, by forming cube-shaped Cu_2O, the GO is dispersed more uniformly, and the GO and the Cu_2O are more tightly combined, which makes a good foundation for subsequent

experiments and performance.

Figure 3c shows the microstructure of the CNT/Cu-Ti composite powder after ball milling and reduction, all cubic powders were turned into nearly spherical particles with a reduced size, and the wrinkled structure of RGO can be observed, indicating a good dispersity and topographic integrity of RGO. XRD investigation shows characteristic peaks of Cu in the patterns, which may be attributed to the low content of RGO (Figure 3d).

Raman spectroscopy shows the structural change of GO in each of the fabrication processes by analysis the intensity ratio of D (~ 1350 cm^{-1}) and G (~ 1600 cm^{-1}) band (Figure 3e). The I_D: I_G value of the starting GO is ~0.83, indicating a certain quantity of defects, which can provide nucleation sites for Cu_2O particles. This ratio is raised to 0.94 for 0.3 wt.%RGO/Cu-Ti powder, inferring that the increased defects RGO during the ball milling process, which still retained even after H_2 reduction. In addition, the G band of 0.3 wt. %RGO/Cu-Ti composite powder is shifted to the high wavenumber by ~10 cm^{-1} compared with that of the GO due to the strong interaction of electrons between Cu_2O and GO, and the powerful electron coupling contributes to the adsorption of Cu_2O by GO [14]. However, the I_D: I_G value is reduced to 0.68 in the composite, suggesting that there barely any new defects were introduced, and the D band vibration was suppressed [15].

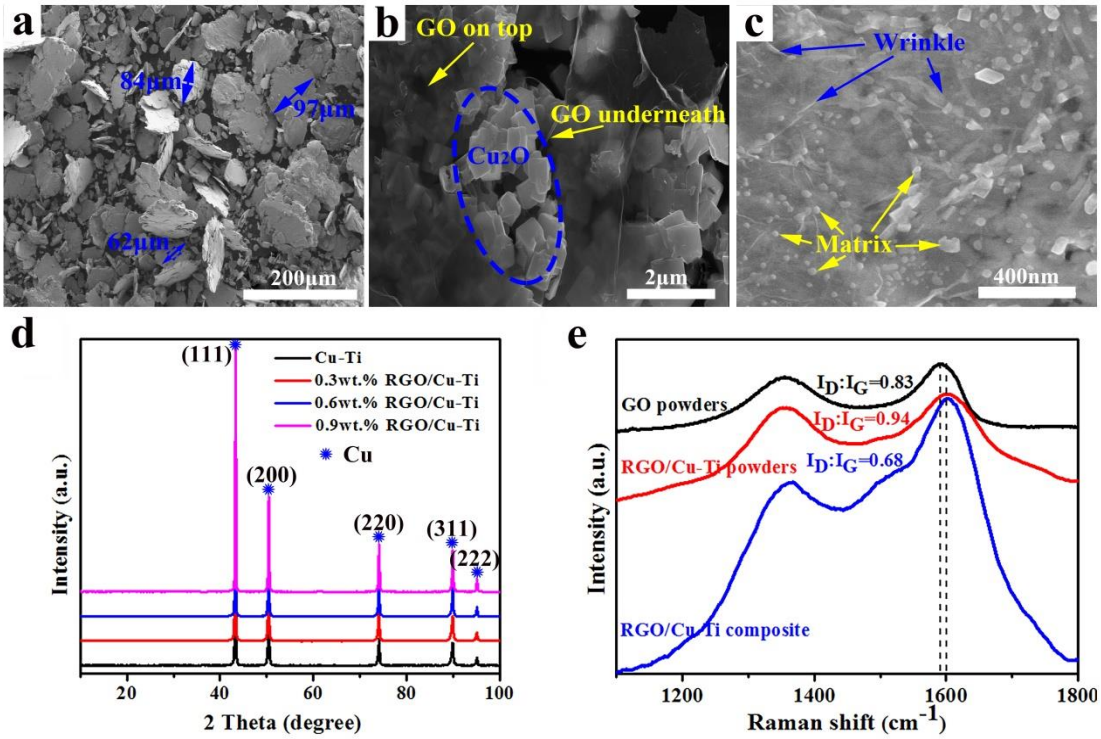

Figure 3. SEM images of (a) Flaked Cu powders; (b) GO/Cu_2O composite powders; (c) RGO/Cu-Ti composite powder; and (d) XRD patterns; (e) Raman spectra.

3.3 Characterization of the 0.3 wt.% RGO/Cu-Ti composite

At the interface of Cu and RGO (Figure 4a), the area labeled by the red arrow indicates the location of the RGO under a bright field. Further magnification of the interface between RGO and Cu in Figure 4b shows a 5-15 nm transition interface instead of a clear and intuitive interface. The FFT images (Figure 4c) of the marked box c reveal the characteristic (220) and (200) diffraction spots of TiC phase. Based on the noise-filtered IFFT image, the lattice inter-planar spacing is measured to be ~0.222 nm, which is perfectly matched to the d-spacing of (200) planes of TiC. Interestingly, different from the green box area, a titanium-carbon compound is found in the blue box which is more close to the matrix (Figure 4d). Based on the FFT and IFFT patterns of the marked areas, the inter-planar spacing of these lattice fringes are measured to be ~0.162 nm and ~0.261 nm, corresponding to the d-spacing of (009) and (021) planes of cubic Ti_8C_5 phase, respectively. It is well known that the interfacial reaction between carbon and Cu binary systems cannot occur [16].

Therefore, the interface bonding between the reinforcement of RGO and the Cu-Ti matrix can be improved by these formed transition carbides. The appearance of the transition phase indicates that titanium atoms have been segregated from the lattice of Cu-1.0Ti alloy, and reacted with carbon atoms with higher activity at the interface.

Phase transformation reactions will occur in the Ti-C system due to the sufficiently high sintering temperature at ~1073K [17]. Based on the HRTEM analysis, a possible formation mechanism of interfacial Ti_xC_y nanophase is put forward (Figure 4e). The titanium-carbon compound will be formed due to the combination of active carbon atoms from rapid diffusion and titanium atoms precipitated from the copper matrix. The Gibbs free energy of Ti_8C_5 is calculated as -280.58 kJ/mol at sintering temperature of 1073K, whereas TiC is -172.23 kJ/mol. However, the diffusion rate of C atoms will be accelerated with the new phase formation. At this point, the previously generated Ti_8C_5 will continue reacting with C to form TiC (the Gibbs free energy is -445.92 kJ/mol). In addition, a phase change from Ti_8C_5 to TiC will occur (Ti_8C_5+3C=8TiC) due to the more stable face-centered structure of the TiC phase [18].

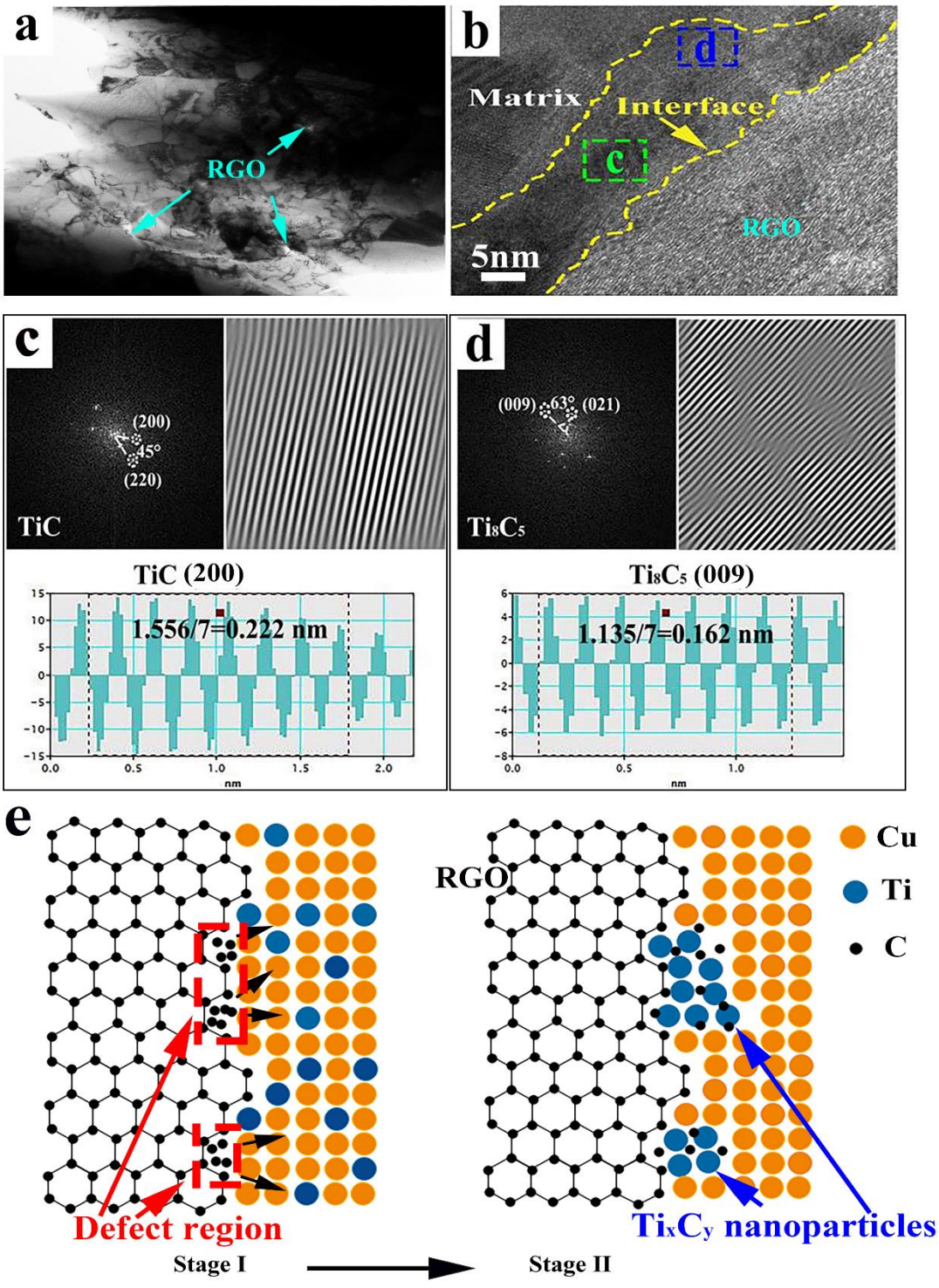

Figure 4. Morphology of the 0.3 wt.% RGO/Cu-Ti composite. (a) TEM image of RGO position in matrix; (b) HRTEM image of the interface I; (c-d) FFT, IFFT and corresponding lattice spacing measurement recorded at the mark c and d regions in (b); (e) Schematics of possible carbide formation mechanism in RGO/Cu-Ti composite.

3.4 Mechanical Properties

The relative density and mechanical properties are summarized in Table 1and Fig.5a, b. The measured hardness, yield strength (YS) and ultimate tensile strength (UTS) of the composite increase to 147.2 HV, 222 MPa and 440 MPa, respectively, when the RGO content is 0.3wt% compared with of the alloy matrix material. And, all of them maintain a high level at 132.7 HV, 215 MPa and 398 MPa, respectively, even to 0.6wt%. However, for the 0.9wt% RGO/Cu-Ti sample, mechanical properties have been severely deteriorated, the relative density is only 97.3% and elongation (EL) is only 3.0%, which are much lower than those of the matrix material.

To better understand the evolution of the mechanical behavior of the composites, the surface is analyzed by SEM (Figure 5). All samples show the ductile fracture properties due to the dimples on the fractural surface. Compared with the fracture morphology of a Cu-Ti composite (Figure 5c), pulled-out RGO can be observed on the fracture surface (Figure 5d-e), suggesting the load from the Cu matrix to the reinforcements during tensile tests. It is clear that detected RGO is adhered and embedded firmly into the metal matrix, which is inseparable from the strong interface bonding. However, relatively large, shallow and fewer dimples appear in 0.9 wt.% samples, showing poor plasticity because of the stress-concentration caused by RGO clusters. These clusters also reduce the relative density, which is consistent with the finding in section 3.2.

Table. 1. Relative density and mechanical properties of composites with different RGO contents.

Samples	Relative density(%)	Hardness (HV)	YS (MPa)	UTS (MPa)	EL (%)
Cu-Ti	98.6	90.3±8	140±5	274±10	11.9±0.3
0.3wt.%RGO	98.8	147.2±3	222±3.5	440±7	10.3±0.4
0.6wt.%RGO	98.4	132.7±2	215±4	398±3	10.6±0.4
0.9wt.%RGO	97.3	80.6±2	130±6	241±8	3.9±0.3

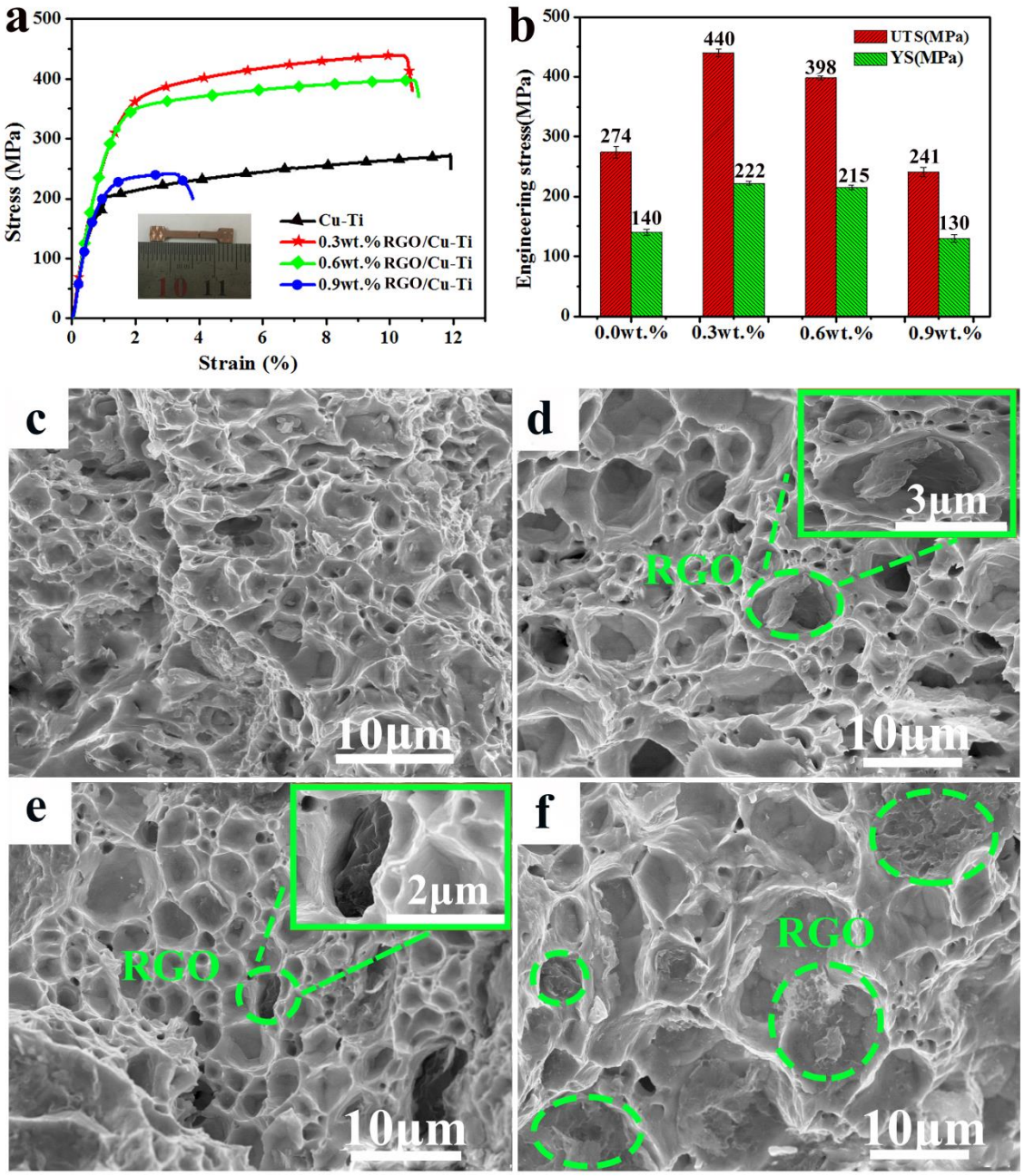

Figure 5. Stress-strain curves and obtained YS/UTS values of the composites (a) and (b); fracture surface morphologies of composites with different content of RGO (c) 0 wt%; (d) 0.3 wt%; (e) 0.6 wt%; (f) 0.9 wt%.

3.5 Strengthening Mechanisms

Strengthening mechanisms, normally, can be discussed as: load transfer strengthening, thermal mismatch strengthening, grain refinement, second phase strengthening. These mechanisms may occur simultaneously during the strengthening process.

It is worth noting that the thermal mismatch strengthening is possible and has already been reported in MMCs when the composite is cooled down at a rapid rate, such as by water quenching [19]. In this research, due to the comparatively low cooling rate, the thermal mismatch effect is ignored. Based on the results of the microstructure analysis, relevant theoretical discussion is given, the relevant calculation formulas and specific assignments can be referred elsewhere [20].

Cu grain boundary migration is hindered by a sufficiently high volume fraction of RGO, which are surrounded at the grain boundaries, resulting in grain refinement in Fig.6. The better dispersed GO can improve the in-situ generation of Ti_xC_y which is beneficial the grains. The strengthening effect of grain reinforcement $\Delta\sigma_{GR}$ can be estimated as ~7.71 MPa from the Hall-Petch relationship [21]. RGO acts as a bridge, and the load in the matrix is effectively transferred according to the fracture surface feature. The strength increased by load transfer $\Delta\sigma_{L.T.}$ estimated by the shear lag model [22] and the measured value is 103.2 MPa.

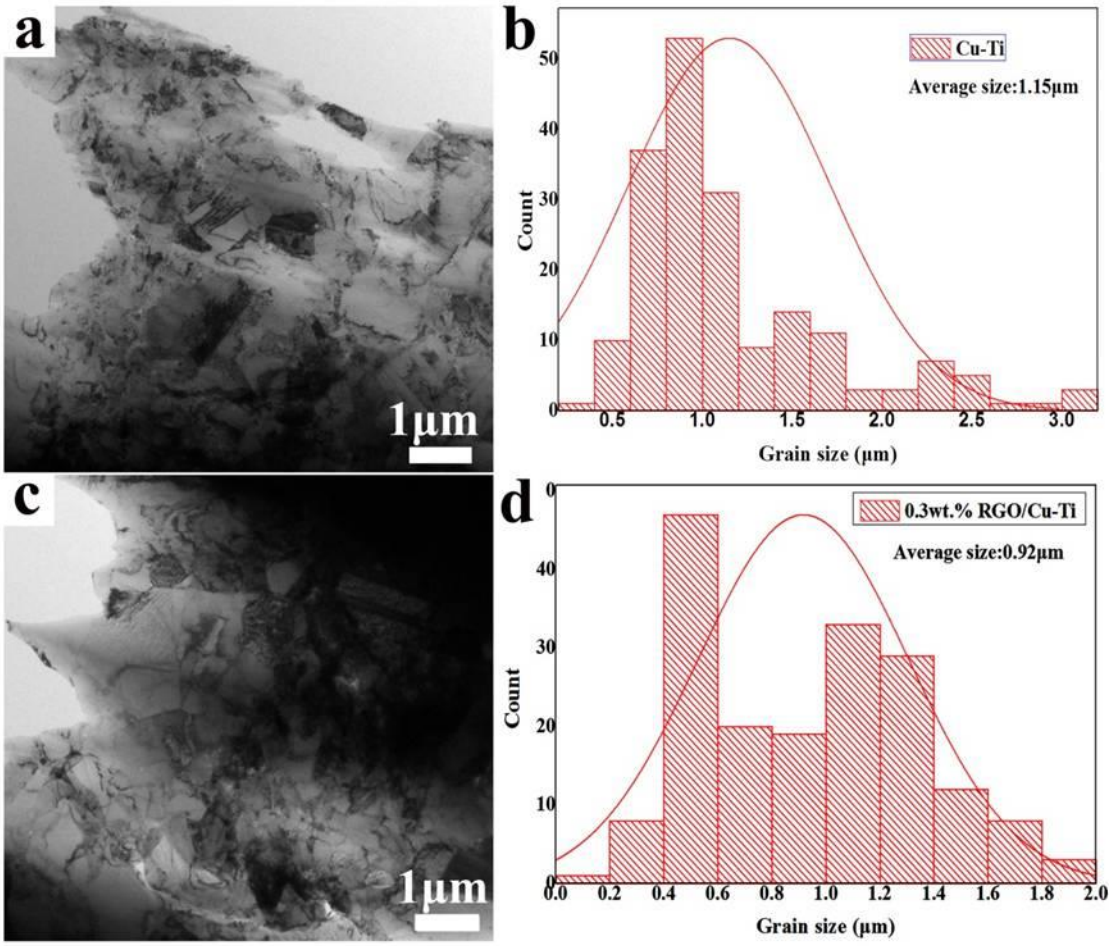

Fig. 6. TEM observations of the average grain size and statistical charts of the composites (a) (b) Cu-Ti; (c) (d) 0.3wt. %RGO/Cu-Ti.

In our study, the strengthening of the second phase cannot be ignored due to the in-situ generated and uniformly dispersed Ti_xC_y nanophases. Adjacent particles accumulate, pinning and forming a dislocation loop, thereby hindering the movement of dislocations and result in reinforcing effect [23]. Therefore, from the analysis of the previous results, it can be known that the carbon source is provided by RGO, and the phase-reversed in-situ reaction with the Ti precipitated in the matrix generates a hard and brittle nano-sized (non-deformable) Ti_xC_y, resulting in a second phase strengthening. The Orowan-Ashby model is used to estimate the second phase enhancement contribution $\Delta\sigma_{S.P}$, which is ~52.31 MPa.

The predicted tensile strength of 0.3 wt.% RGO/Cu-Ti is 437.2 MPa by summing up the $\Delta\sigma_{GR}$, $\Delta\sigma_{L.T.}$ and $\Delta\sigma_{S.P.}$ (Figure 7a). This calculated value is close to the

experimental value, confirming that the three enhancements analyzed above are valid. Obviously, load transfer is the major contributor to effect. The high load transfer efficiency *R* of RGO/Cu-Ti composite is evidenced by the strong interfacial bonding. Figure 7b summarizes the *R* versus volume of reinforcement V_f obtained from the present RGO/Cu-Ti composite and those reported for related composites prepared by five typical methods including molecular-level mixing [24], in-situ growth of graphene on Cu powders [25, 26], high-energy ball-milling [5], ball-milling and high-ratio rolling [27] and CNT-GR hybrids reinforcement in Cu matrix composite [28]. In this study, the composites prepared by our strategy realize a good balance of *R* and V_f, due to a good combination of the GO with the matrix material, and the firm interface bonding by the formation of the second phase. From comparison, it can be found that the *R* in our study is more accurate to the optimal *R* value achieved by molecular mixing and in situ on the surface of Cu powder.

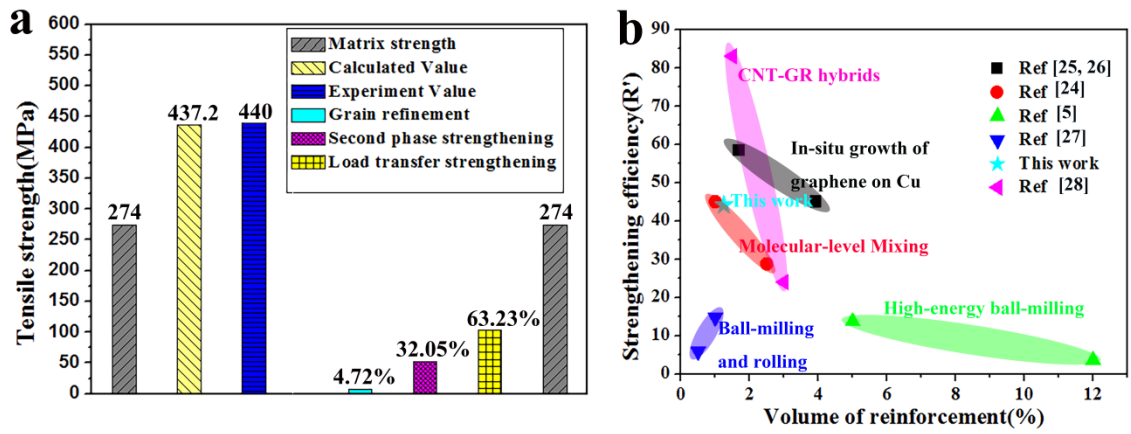

Figure 7. (a) Tensile strength of matrix strength, experimental value and calculated value (left part) and strengthening contributions (right part); (b) Reinforcing efficiency (R) of the composites.

4. Conclusions

(1) A strategy of RGO/Cu−Ti composites preparation based on the electrostatic adsorption is achieved.

(2) The obtained composites have well dispersed and distributed RGO in the matrix.

(3) Interface bonding is improved by the in-situ formed carbide nanoparticles, which acts as load transfer bridges. Nucleation and growth of the carbides like Ti_8C_5 and TiC occur from the precipitation and diffusion of Ti atoms in the carbon area.

(4) The as-fabricated RGO/Cu−Ti composite exhibits a significant enhancement in tensile strength and strengthening efficiency.

Acknowledgement

This work is supported by National Natural Science Foundation of China (51861014 & 51864029), Major projects of Yunnan Provincial Department of Education (2016CYH08) and Innovation team of Yunnan Provincial Science and Technology Department (2017HC033).

References

[1] NIETO Andy, BISHT Ankita, LAHIRI Debrupa, ZHANG Cheng, AGARWAL Arivind. Graphene reinforced metal and ceramic matrix composites: a review[J]. International Materials Reviews, 2016;62:241-302.
[2] GAO Xin, YUE Hong-yue, GUO Erjun, ZHANG Hong, LIN Xuan-yu, YAO Long-hui, WANG Bao. Mechanical properties and thermal conductivity of graphene reinforced copper matrix composites[J]. Powder Technology, 2016;301:601-7.
[3] ADAMSKA Lyudmyla, LIN You, ROSS Andrew J, BATZILL Matthias, OLEYNIK Ivan I. Atomic and electronic structure of simple metal/graphene and complex metal/graphene/metal interfaces[J]. Physical Review B Condensed Matter, 2012;85:2202-8.
[4] JIANG Rong-rong, ZHOU Xu-feng, FANG Qi-le, LIU Zhao-ping. Copper–graphene bulk composites with homogeneous graphene dispersion and enhanced mechanical properties[J]. Materials Science and Engineering: A, 2016;654:124-30.
[5] CHU Ke, JIA Cheng-cheng. Enhanced strength in bulk graphene-copper composites[J]. physica status solidi (a), 2014;211:184-90.
[6] LIU Liang, BAO Rui, YI Jian-hong. Mono-dispersed and homogeneous CNT/Cu composite powder preparation through forming Cu 2 O intermediates[J]. Powder Technology, 2018;328:430-5.
[7] CHO Seung-chan, KIKUCHI Keiko, MIYAZAKI Takamichi, KAWASAKI Akira, ARAMI Yoshiro, SILVAIN Jean-francois. Epitaxial growth of chromium carbide nanostructures on multiwalled carbon

nanotubes (MWCNTs) in MWCNT–copper composites[J]. Acta Materialia, 2013;61:708-16.
[8] ZHANG Xin-jiang, DAI Zhong-kui, LIU Xue-ran, YANG Wen-chao, HE Meng, YANG Zi-run. Microstructural Characteristics and Mechanical Behavior of Spark Plasma-Sintered Cu–Cr–rGO Copper Matrix Composites[J]. Acta Metallurgica Sinica, 2018:1-10.
[9] ZHANG Xin, WAN Dong-qin, PENG Kun, ZHANG Wei. Enhancement of Thermal Conductivity and Mechanical Properties of Cu-Reduced Graphene Oxide Composites by Interface Modification[J]. Journal of Materials Engineering and Performance,28(8),2019,5165-5171.
[10] YANG Zi-yue, WANG Li-dong, SHI Zhen-dong, WANG Miao, CUI Ye, WEI Bing, XU Shi-chong, ZHU Yin-peng, FEI Wei-dong. Preparation mechanism of hierarchical layered structure of graphene/copper composite with ultrahigh tensile strength[J]. Carbon, 2018;127:329-39.
[11] LUO Hai-bo, SUI Yan-wei, QI Ji-qiu, MENG Qing-kun, WEI Fu-xiang, HE Ye-zeng. Mechanical enhancement of copper matrix composites with homogeneously dispersed graphene modified by silver nanoparticles[J]. J Alloy Compd,2017;729:293-302.
[12] HE Ye-zeng, WANG Shi-tong, LUO Hai-bo, WANG Cong. Ag-rGO content dependence of the mechanical, conductive and anti-corrosion properties of copper matrix composites[J]. Materials Research Express,5:096523-.
[13] LUO Hai-bo, SUI Yan-wei, QI Ji-qiu, MENG Qing-kun, WEI Fu-xiang, HE Ye-zeng. Copper matrix composites enhanced by silver/reduced graphene oxide hybrids[J]. Materials Letters, 2017;196:354-7.
[14] CHU Ke, WAMG Fan, LI Yu-biao, WANG Xiao-hu, HUANG Da-jian, GENG Zhong-rong. Interface and mechanical/thermal properties of graphene/copper composite with Mo 2 C nanoparticles grown on graphene[J]. Composites Part A Applied Science & Manufacturing,S1359835X18301167.
[15] GUO Bai-song, SONG Min, YI Jian-hong, NI Song, SHEN Tao, DU Yong. Improving the mechanical properties of carbon nanotubes reinforced pure aluminum matrix composites by achieving non-equilibrium interface[J]. Materials & Design, 2017;120:56-65.
[16] LIU Liang, BAO Rui, YI Jian-hong, LI Cai-ju, TAO Jing-mei, LIU Yi-chun, TANG song-lin,YOU xin. Well-dispersion of CNTs and enhanced mechanical properties in CNTs/Cu-Ti composites fabricated by Molecular Level Mixing[J]. J Alloy Compd, 2017;726:81-7.
[17] WANG Femg-lin, LI Yun-ping, CHIBA Akihiko. Effects of carbon content and size on Ti-C reaction behavior and resultant properties of Cu-Ti-C alloy system[J]. Materials Characterization,2018;141:186-92.
[18] XIONG Ni, BAO Rui,YI Jian-hong,FANG Dong,TAO Jing-mei,LIU Yi-chun. CNTs/Cu-Ti composites fabrication through the synergistic reinforcement of CNTs and in situ generated nano-TiC particles[J]. J Alloy Compd, 2018;S092583881832989X-.
[19] MILLER Ws, HUMPHREYS FJ. Strengthening mechanisms in particulate metal matrix composites[J]. Scripta Metallurgica Et Materialia,1991;25:33-8.
[20] CHEN Xiao-feng, TAO Jing-mei, LIU Yi-chun, BAO Rui, LI Feng-xian, LI Cai-ju, YI Jian-hong. Interface interaction and synergistic strengthening behavior in pure copper matrix composites reinforced with functionalized carbon nanotube-graphene hybrids[J]. Carbon, 2019;146:736-755.
[21] DONG H-nam, CHA Seung-i, LIM Byung K, PARK Hoon M, HAN Do S, HONG Song H. Synergistic strengthening by load transfer mechanism and grain refinement of CNT/Al–Cu composites[J]. Carbon,2012;50:2417-23.
[22] ZHANG Z, CHEN D-l. Consideration of Orowan strengthening effect in particulate-reinforced metal matrix nanocomposites: A model for predicting their yield strength[J]. Scripta Materialia,

2006;54:1321-6.
[23] GEORGE R, KASHYAP K-T, RAHUL R, YAMDAGBI S. Strengthening in carbon nanotube/aluminium (CNT/Al) composites[J]. Scripta Materialia, 2005;53:1159-63.
[24] HWANG Jaewon, YOON Taeshik, JIN Sung-hwan, LEE Jin-sup, KIM Taek-soo, HONG Soon-hyung, SEOKWOO Jeon. Enhanced mechanical properties of graphene/copper nanocomposites using a molecular-level mixing process[J]. Advanced materials, 2013;25:6724-9.
[25] CHEN Ya-kun, ZHANG Xiang, LIU En-zuo, HE Chun-nian, SHI Chun-sheng, LI Jia-jun, NASH Philip, ZHAO Nai-qin. Fabrication of in-situ grown graphene reinforced Cu matrix composites[J]. Scientific reports, 2016;6:19363.
[26] CHEN Ya-kun, ZHANG Xiang, LIU En-zuo, HE Chun-nian, HAN Ya-jing, LI Qun-ying, NASH Philip, ZHAO Nai-qin. Fabrication of three-dimensional graphene/Cu composite by in-situ CVD and its strengthening mechanism[J]. Journal of Alloys & Compounds, 2016;688:69-76.
[27] KIM WJ, LEE TJ, HAN SH. Multi-layer graphene/copper composites: Preparation using high-ratio differential speed rolling, microstructure and mechanical properties[J]. Carbon, 2014;69:55-65.
[28] YOO SJ, HAN SH, KIM WJ. A combination of ball milling and high-ratio differential speed rolling for synthesizing carbon nanotube/copper composites[J]. Carbon, 2013;61:487-500.
[29] SI Xiao-yang, LI Mian, CHEN Fan-yan, EKLUND Per, XUE Jian-ming, HUANG feng, DU Shi-yu, HUANG Qing. Effect of carbide interlayers on the microstructure and properties of graphene-nanoplatelet-reinforced copper matrix composites[J]. Materials Science and Engineering: A,2017;708:311-8.